EGR1 regulates IGF-1-stimulated pancreatic cancer cell invasion by increasing IL-11 expression

YENA CHOI[1], EUITAEK JUNG[1], JUNEKYU HAN[1] and SOON YOUNG SHIN[1,2]

[1]Department of Biological Sciences, College of Life Science, Konkuk University, Seoul 05029, Republic of Korea; [2]Cancer and Metabolism Institute, Konkuk University, Seoul 05029, Republic of Korea

Received March 3, 2026; Accepted July 23, 2026

DOI: 10.3892/ol.2026.15815

Abstract. Interleukin-11 (IL-11), a member of the glycoprotein-130 cytokine family, has been implicated in inflammation-associated malignancies, including pancreatic cancer, where both IL-11 and its receptors are frequently overexpressed; however, the transcriptional mechanisms that regulate IL-11 expression remain unclear. To investigate this mechanism, promoter reporter assays, electrophoretic mobility shift assays, EGR1 knockdown experiments, gene expression analyses and three-dimensional spheroid invasion assays were performed in pancreatic cancer cells. In the present study, early growth response 1 (EGR1) was identified as a key regulator of insulin-like growth factor 1 (IGF-1)-induced *IL11* transcription. Promoter analyses revealed a conserved EGR1-binding sequence (EBS) within the proximal *IL11* promoter that is essential for IGF-1-responsive transcriptional activation. Electrophoretic mobility shift assays demonstrated that EGR1 directly binds to this site. Functional silencing of EGR1 markedly attenuated IGF-1-induced IL-11 expression and reduced invasive behavior in a three-dimensional pancreatic cancer spheroid model. Collectively, these findings delineated an IGF-1/EGR1/IL-11 signaling axis linking growth factor-dependent transcriptional regulation to invasive phenotypes and highlighted a potential therapeutic target in pancreatic cancer.

Correspondence to: Professor Soon Young Shin, Department of Biological Sciences, College of Life Science, Konkuk University, 120 Neungdong-ro, Gwangjin-gu, Seoul 05029, Republic of Korea
E-mail: shinsy@konkuk.ac.kr

Abbreviations: EGR1, early growth response 1; EBS, EGR1-binding sequence; ELISA, enzyme-linked immunosorbent assay; EMSA, electrophoretic mobility shift assay; EMT, epithelial-to-mesenchymal transition; ERK, extracellular signal-regulated kinase; IGF-1, insulin-like growth factor 1; IL-11, interleukin-11; IL11R, IL-11 receptor; mtEBS, mutated EBS; MAPK, mitogen-activated protein kinase; RT-PCR, reverse transcription-PCR; qPCR, quantitative PCR; shRNA, short hairpin RNA; shCT, control shRNA; shEgr1, EGR1 shRNA

Key words: EGR1, IGF-1, Il-11, pancreatic cancer, invasion

Introduction

Interleukin-11 (IL)-11 is a pleiotropic cytokine in the IL-6 family that signals through the Janus kinase/signal transducer and activator of transcription (JAK/STAT) pathway (1). Although initially characterized for its role in hematopoiesis, IL-11 is now recognized as a contributor to the pathogenesis of multiple solid tumors, including gastrointestinal and bone cancers, where it promotes tumor growth, invasion and metastasis (2). IL-11 binds to its transmembrane receptor, IL-11 receptor α (IL-11Rα), which then associates with the common glycoprotein-130 subunit, leading to activation of the downstream JAK/STAT3, mitogen-activated protein kinase (MAPK)/extracellular signal-regulated kinase (ERK) and phosphoinositide 3-kinase/AKT signaling pathways (3). Through these cascades, IL-11 drives tumorigenesis by inducing epithelial-mesenchymal transition (EMT), angiogenesis, metastasis and modulation of immune responses, making the IL-11 signaling axis an attractive therapeutic target across cancer types (3). However, the regulatory mechanisms underlying *IL11* gene expression during tumor progression remain incompletely understood.

Oncogenic *RAS* mutations occur in 10-30% of human cancers and in >90% of pancreatic ductal adenocarcinomas (PDACs), where they drive aberrant cytokine signaling and tumor progression (4). Pancreatic cancer progression is driven by intricate signaling networks and dynamic interactions within the tumor microenvironment, which collectively promote aggressive phenotypes and therapeutic resistance (5-7). Within this framework, growth factor-mediated signaling pathways have emerged as notable regulators of tumor progression and invasion. In particular, insulin-like growth factor 1 (IGF-1) signaling has been implicated in promoting invasive behavior (8), although the downstream transcriptional mechanisms linking IGF-1 to pro-invasive gene expression remain incompletely defined.

IL-11 expression is regulated by oncogenic RAS signaling through the activator protein-1 (AP-1) transcription factor (9). However, mutation of the AP-1 site within the *IL11* promoter does not completely abolish promoter activity, suggesting the presence of additional cis-acting regulatory sequences. Based on bioinformatic analysis using the JASPAR database (10), a putative EGR1-binding sequence (EBS) was identified between -75 and -48 of the *IL11* promoter. Early growth response 1

(EGR1) is a zinc-finger transcription factor rapidly induced by mitogens and cellular stress, and it regulates diverse cytokines and chemokines (11-14). EGR1 exhibits context-dependent functions in cancer, acting as either a tumor suppressor or an oncogene. In colon, prostate and breast cancers, elevated EGR1 expression is associated with tumor progression, invasion and poor prognosis through regulation of genes involved in cell cycle control, apoptosis and angiogenesis (15-17). Nevertheless, the specific contribution and downstream targets of EGR1 in *IL11* expression remain unclear.

In the present study, we hypothesized a linear signaling axis in which the transcription factor EGR1 mediates IL-11 upregulation and promotes cancer cell invasion. The study aimed to elucidate the functional role and transcriptional mechanism of the IGF-1/EGR1/IL-11 axis in pancreatic cancer. Elucidation of this IGF-1/EGR1/IL-11 signaling cascade will provide insights into the molecular drivers of pancreatic cancer metastasis and identify potential therapeutic targets.

Materials and methods

Cell culture. Capan-1 (human pancreatic carcinoma, KRAS/G12V), MIA PaCa-2 (human pancreatic carcinoma, KRAS/G12C), MDA-MB-231 (breast carcinoma, KRAS/G13D), HT1080 (fibrosarcoma, NRAS/C181A), SW480 and SW620 (colon carcinoma, KRAS/G12V), HeLa (cervical carcinoma), 293 (embryonic kidney) and MCF7 (breast carcinoma) cells were obtained from the American Type Culture Collection. Cells were cultured in Dulbecco's modified Eagle's medium (DMEM; Welgene Inc.) supplemented with 10% fetal bovine serum (FBS; Gibco; Thermo Fisher Scientific, Inc.), 100 U/ml penicillin and 100 μg/ml streptomycin (Welgene Inc.) at 37˚C in 5% CO_2.

Reagents. IGF-1 was purchased from R&D Systems Inc., and epidermal growth factor (EGF), basic fibroblast growth factor (bFGF) and platelet-derived growth factor (PDGF) were obtained from PeproTech, Inc.. Recombinant human EGR1 protein expressed in Sf9 insect cells was purchased from MilliporeSigma. A neutralizing antibody to IL-11Rα was obtained from Santa Cruz Biotechnology Inc..

Generation of IL11 promoter-reporter construct. The human *IL11* promoter was cloned into the pGL3-Basic vector (Promega Corporation) as previously described (9). Site-directed mutagenesis of the EBS was performed using a mutagenesis kit (cat. no. EZ004M; Enzynomics Co., Ltd.). The AP-1 binding site mutant construct was generated as previously reported (9).

Transfections and IL11 promoter reporter assay. Capan-1 cells cultured in a 24-well plate were transfected with wild-type or mutant *IL11* promoter-reporter constructs (0.1 μg each) using Lipofectamine 2000 (Thermo Fisher Scientific, Inc.) and incubated for 24 h at 37˚C. Following this 24-h post-transfection interval, the cells were stimulated with 100 ng/ml IGF-1 for an additional 12 h at 37˚C, after which they were harvested and lysed using Reporter Lysis buffer (Promega Corporation) for luciferase activity measurement. To evaluate the effects of EGR1 and Fos-related antigen 1 (FRA-1) on *IL11* promoter activity, Capan-1 cells were co-transfected with 0.1 μg of pIL11-Luc(-153/+14) and 0.1 μg each of expression vectors encoding EGR1 (NM_007913.5) and/or FRA-1 (NM_005438.5), which were subcloned into the pcDNA3.1 vector (Thermo Fisher Scientific, Inc.), using Lipofectamine LTX with PLUS Reagent (Thermo Fisher Scientific, Inc.). The total plasmid concentration transfected was adjusted to 0.2 μg using an empty pcDNA3.1 vector. To control for transfection efficiency, all samples included 50 ng of pRL-null plasmid encoding *Renilla* luciferase (Promega Corporation). Following transfection, the cells were maintained for 48 h at 37˚C in a humidified incubator containing 5% CO_2, after which they were harvested and lysed using Reporter Lysis Buffer (Promega Corporation). Luciferase activities were measured using the Dual-Luciferase® Reporter Assay System (Promega Corporation,) according to the manufacturer's protocol. Briefly, cells were washed twice with ice-cold phosphate-buffered saline (PBS) and lysed in 100 μl 1X Passive Lysis Buffer by shaking gently at room temperature for 15 min. Cell lysates were cleared by centrifugation at 12,000 x *g* for 5 min at 4˚C, and 20 μl of the supernatant was transferred to a luminometer tube. Firefly luciferase activity was initiated by adding 100 μl Luciferase Assay Reagent II (LAR II), and luminescence was recorded on a GloMax 20/20 Luminometer (Promega Corporation). Next, 100 μl Stop & Glo Reagent (Promega Corporation) was added to simultaneously quench Firefly luminescence and activate *Renilla* luciferase, followed immediately by a second luminescence reading using the same measurement parameters. Relative promoter activity was determined by normalizing Firefly luciferase relative light units (RLU) to *Renilla* luciferase RLU (Firefly RLU/*Renilla* RLU). Promoter-reporter luciferase activities were expressed as a fold change relative to the control group, which was set to 1.

Gene silencing. Lentiviral short hairpin RNA (shRNA) constructs targeting human EGR1 (shEGR1; TRCN_0000273850; MISSION shRNA) and non-targeting control shRNA (shCT; SHC016V; MISSION Lentiviral Controls) were purchased from MilliporeSigma. The shRNA constructs were cloned into the pLKO.1-puro lentiviral vector backbone (MilliporeSigma). Lentiviral transduction was performed according to the manufacturer's protocol as previously described (18). Cells were incubated with lentiviral particles at 37˚C in a humidified 5% CO_2 atmosphere for 24 h, then replaced with fresh culture medium. Stably transfected clones were subsequently selected using puromycin (cat. no. ant-pr-1; InvivoGen). Briefly, cells were infected with lentivirus on day 0, the medium was replaced on day 1, puromycin selection (1 μg/ml) was performed from days 2-4, and all subsequent experiments were conducted on day 5. Knockdown efficiency was confirmed by immunoblotting.

Cell treatment with MAPK inhibitors. Capan-1 cells were pre-treated with U0126 (cat. no. 9930; Cell Signaling Technology, Inc.), SP600125 (cat. no. S1460; Selleck Chemicals) or SB203580 (cat. no. 1202; Tocris Bioscience) at a final concentration of 10 μM (prepared from 10 mM stock solutions at a 1:1,000 dilution) for 30 min at 37˚C, followed by IGF-1 (100 ng/ml) treatment. The cells were harvested after 90 min for immunoblot analysis and after 18 h for quantitative PCR (qPCR) analysis.

Reverse-transcription PCR (RT-PCR). To determine the steady-state mRNA levels of *IL11* and *IL11R* across various cell lines, total RNA was extracted using NucleoZOL (MACHEREY-NAGEL GmbH & Co. KG) according to the manufacturer's instructions. RNA concentration and purity were assessed using a NanoDrop spectrophotometer (Omega BioTek, Inc.). cDNA was synthesized using the CellSafe Master cDNA Synthesis Mix (CellSafe Co., Ltd.) and adjusted to a final concentration of 100 ng/μl. The resulting cDNA preparations were used as templates for RT-PCR analysis. PCR gene-specific primer sequences for *IL11* (NM_000641), *IL11R* (NM_ 001142784.3) and *GAPDH* (NM_002046.7) were as follows: *IL11* forward, 5'-ACTGCTGCTGCTGAAGACTCGGCTGTG-3' and reverse, 5'-ATGGGGAAGAGCCAGGGCAGAAGTCTGT-3'; *IL11R* forward, 5'-GCCAAGCAGCCGACTATGAGAA-3' and reverse, 5'-AGTAGCCGAGGGTGTGGTTGGA-3'; and *GAPDH* forward, 5'-ACCCACTCCTCCACCTTTG-3' and reverse, 5'-CTCTTGTGCTCTTGCTGGG-3'. The PCR reaction was conducted in a total volume of 20 μl, including 10 μl 2X PCR master mix (cat. no. MC-E-005-5; Macrogen), 1 μl forward primer (10 pmol/μl), 1 μl reverse primer (10 pmol/μl), 1 μl template cDNA and 7 μl nuclease-free water. The final concentration of each primer in the reaction mixture was 0.5 μM. PCR amplification was performed using a hot-start Taq polymerase with an initial activation at 95˚C for 5 min, followed by 30 cycles of denaturation at 95˚C for 30 sec, annealing at 55˚C for 30 sec and extension at 72˚C for 1 min, with a final extension at 72˚C for 5 min. Amplified products were resolved on 2% agarose gels containing 0.5 μg/ml ethidium bromide (cat. no. H5041; Promega Corporation) and visualized under UV illumination using an Axygen gel documentation system GD-1000 (Axygen Biosciences). Ethidium bromide was incorporated into the agarose gels before electrophoresis; therefore, no separate post-electrophoresis staining step was performed.

Quantitative real-time PCR (qPCR). To quantify *IL11* mRNA expression by qPCR, Capan-1 cells were serum-starved in media containing 0.5% FBS for 18 h, and then treated individually with vehicle (PBS), 10% FBS, 20 ng/ml EGF, 50 ng/ml FGF, 50 ng/ml PDGF or 100 ng/ml IGF-1 for 18 h at 37˚C. In some experiments, Capan-1 cells were pretreated with the indicated inhibitors as described in the section 'Cell treatment with MAPK inhibitors'.

The resulting cDNA preparations were used as templates for qPCR analyses. Following treatment, cells were harvested, and total RNA extraction and cDNA synthesis were performed as described in the section on RT-PCR.

The relative expression levels of *IL11* mRNA were measured by qPCR using a CFX96 Real-Time PCR Detection System (Bio-Rad Laboratories, Inc.). Each 20-μl reaction contained 100 ng of cDNA template, 5 pmol of each gene-specific primer (final concentration, 0.25 μM), 1X reaction buffer (cat. no. P725; Enzynomics) containing 0.5 units Hot-Taq DNA polymerase and dNTPs, and 0.5X SYBR Green I nucleic acid stain (cat. no. HY-K1004; MedChemExpress), corresponding to a 1:20,000 dilution of the 10,000X stock solution. The thermocycling conditions consisted of an initial denaturation at 95˚C for 10 min, followed by 45 cycles of denaturation at 95˚C for 20 sec, annealing at 60˚C for 20 sec and extension at 72˚C for 30 sec. The qPCR primers for *IL11* (NM_000641) and *ACTB* (NM_001101.5) were as follows: *IL11* forward, 5'-GGACCACAACCTGGATTCCCTG-3' and *IL11* reverse, 5'-AGTAGGTCCGCTCGCAGCCTT-3'; *ACTB* forward, 5'-CACCATTGGCAATGAGCGGTTC-3' and *ACTB* reverse, 5'-AGGTCTTTGCGGATGTCCACGT-3'. Relative *IL11* mRNA expression was calculated using the $2^{-\Delta\Delta Cq}$ method (19), with *ACTB* as the endogenous control. The forward and reverse primers for *ACTB* target a highly conserved nucleotide sequence shared between *ACTB* (β-actin) and *ACTG1* (γ-cytoplasmic actin). This design was intentionally employed to capture the entire cytoplasmic actin transcript pool, thereby buffering against minor, treatment-induced fluctuations in expression of a single actin isoform and providing a more robust normalization baseline. The reference signal using these *ACTB* primers remained stable across all experimental conditions, as confirmed by consistent Cq values and a single melting curve peak, supporting their suitability as an internal reference for normalization. The *IL11* amplicon length was 102 base pairs.

Immunoblotting. Whole-cell lysates were prepared using a laboratory-prepared high-salt radioimmunoprecipitation assay buffer containing 50 mM Tris-HCl (pH 7.4), 400 mM NaCl, 1% Triton X-100, 0.25% sodium deoxycholate, 1 mM EDTA, 1 mM sodium orthovanadate, 1 mM NaF and 0.1% sodium azide. The buffer was supplemented immediately before use with phenylmethanesulfonyl fluoride and protease and phosphatase inhibitor cocktails. Protein concentrations were determined using an EZ-BCA Protein Quantification Kit (cat. no. DG-BCA500; DoGenBio). Depending on the target protein, 10 μg of total protein per lane A total of 10 μg of protein was loaded per lane and was separated on 8% SDS-polyacrylamide gels and transferred onto 0.45-μm nitrocellulose membranes as previously described (20). The membranes were incubated with primary antibodies overnight at 4˚C. The following primary antibodies were used: FRA-1 (1:1,000; cat. no. sc-183; Santa Cruz Biotechnology, Inc.), EGR-1 (1:10,000; cat. no. ab194357; Abcam), Lamin B1 (1:1,000; cat. no. sc-6216; Santa Cruz Biotechnology, Inc.) and GAPDH (1:6,000; cat. no. sc-32233; Santa Cruz Biotechnology, Inc.). The FRA-1 and EGR-1 antibodies were diluted in Tris-buffered saline containing 0.05% Tween 20 (TBST) and 2.5% bovine serum albumin (BSA; cat. no. BSAS 0.1; BovoStar, Bovogen Biologicals), whereas the GAPDH antibody was diluted in TBST containing 5% skimmed milk. Membranes were then incubated with horse radish peroxidase (HRP)-conjugated secondary antibodies for 1 h at 25˚C (1:5,000; diluted in 2.5% BSA in TBST). The following secondary antibodies were used: goat anti-Rabbit IgG (H+L)-HRP (cat. no. 31460; Invitrogen, Thermo Fisher Scientific, Inc.), goat anti-mouse IgG (H+L)-HRP (cat. no. 31430; Invitrogen; Thermo Fisher Scientific, Inc) and rabbit anti-goat IgG (H+L)-HRP (cat. no. 31402; Invitrogen; Thermo Fisher Scientific, Inc). Protein bands were visualized using WestGlow PICO PLUS ECL Chemiluminescent Substrate (cat. no. BWP0200; Biomax) or WestGlow ECL Chemiluminescent Substrate (cat. no. BWE0200; Biomax), depending on signal intensity. Chemiluminescent images were acquired using a ChemiDoc MP Imaging System (Bio-Rad Laboratories, Inc.). Relative band intensities were quantified using ImageJ software (version 1.52a; National Institutes of Health).

Electrophoretic mobility shift assay (EMSA). Purified EGR1 proteins were incubated with biotin-labeled EBS oligonucleotide probe corresponding to positions -48 to -32 (5'-biotin-CGCCCGCCCCAGCCCCC-3'; Bioneer) at room temperature for 20 min. Protein-DNA complexes were detected using a Chemiluminescent Nucleic Acid Detection Module (cat. no. 89880; Thermo Fisher Scientific, Inc.) according to the manufacturer's instructions (20). For fluorescent EMSA using nuclear extracts, complementary oligonucleotides synthesized by Bionics were annealed to generate a double-stranded probe containing the consensus EBS sequence (5'-GGATCCAGC GGGGGCGAGCGGGGGCGA-3'). The sense strand was labeled at the 5' end with 6-carboxyfluorescein (6-FAM). Nuclear extracts were prepared using a hypotonic swelling followed by high-salt extraction. Briefly, nuclear extracts were prepared by hypotonic swelling followed by detergent permeabilization and high-salt extraction, as previously described (20), with minor modifications. Briefly, cells were resuspended in a hypotonic lysis buffer [10 mM HEPES-NaOH (pH 7.5), 10 mM KCl, 1.5 mM $MgCl_2$, 0.1 mM EGTA and 0.4% Triton X-100] and incubated on ice for 30 min. Following centrifugation at 15,000 x g for 10 min at 4˚C, the pellet was resuspended in extraction buffer [20 mM HEPES-NaOH (pH 7.5), 400 mM NaCl, 1.5 mM $MgCl_2$, 0.1 mM EGTA and 0.1% Triton X-100] and incubated on ice for 15 min. After centrifugation at 15,000 x g for 15 min at 4˚C, the supernatant containing the nuclear extract was collected and stored on ice until use. Protein concentrations were determined using a bicinchoninic acid assay kit (cat. no. DG-BCA500; DoGenBio). A total of 3 μg of nuclear extract was incubated with the 5'-6-FAM-labeled double-stranded EGR1 consensus probe (300 fmole) in binding buffer for 20 min at 25˚C prior to electrophoresis. DNA-protein complexes were resolved on a 6% non-denaturing polyacrylamide gel in 0.5X TBE buffer under native conditions. Electrophoresis was performed at 100 V for 40 min at 25˚C. Fluorescent signals were detected using a ChemiDoc MP imaging system (Bio-Rad Laboratories, Inc.) with Alexa Fluor 488 detection settings.

Enzyme-linked immunosorbent assay (ELISA). Secreted IL-11 levels in the culture medium were measured using a Human IL-11 Quantikine ELISA Kit (cat. no. D1100; R&D Systems, Inc.). Capan-1 cells were seeded in 6-well plates and treated with the indicated agents. After 24 h, the culture medium was collected, centrifuged to remove cellular debris, and analyzed using ELISA according to the manufacturer's instructions. Absorbance was measured at 450 nm using the Synergy™ HTX Multi-Mode Microplate Reader (Bio Tek Instruments, Inc.).

Transwell cell invasion assay. A Transwell cell invasion assay was performed using the CytoSelect™ 24-well Cell Migration and Invasion assay kit (Basement membrane, 8 μm pore size; colorimetric format; cat. no. CBA-100-C; Cell Biolabs, Inc.) according to the manufacturer's instructions. Capan-1 cells were serum-starved in medium containing 0.5% FBS for 24 h. Serum-starved Capan-1 cells ($1x10^5$/well) were seeded into inserts commercially pre-incubated with a uniform layer of dried basement membrane matrix. Cells seeded in the upper chamber were treated with IGF-1 (100 ng/ml), IL-11 (10 ng/ml) or IGF-1 (100 ng/ml) plus anti-IL-11Rα antibody (2 μg/ml). Both the upper and lower chambers contained serum-free medium throughout the assay. After 24 h at 37˚C, the remaining non-invasive cells in the upper chamber were removed with a cotton swab, and the invading cells that passed through the basement membrane layer at the bottom of the insert membrane were fixed with 4% paraformaldehyde for 10 min at 25˚C, stained with 0.1% crystal violet for 15 min at 25˚C, washed thoroughly with distilled water, air-dried, and imaged using an EVOS FL fluorescence microscope (Advanced Microscopy Group).

Three-dimensional spheroid sprouting assay. Capan-1 transfectants expressing shCT or shEgr1 were maintained in DMEM (Welgene, Inc.) supplemented with 10% fetal bovine serum (Thermo Fisher Scientific, Inc.) and penicillin-streptomycin (Welgene, Inc.) at 37˚C in a humidified incubator with 5% CO_2. For spheroid formation, cells were resuspended at a density of 2,000 cells per 25 μl in spheroid-forming medium consisting of 80% DMEM, 8% FBS, 0.8% penicillin-streptomycin and 20% Methocel (Thermo Fisher Scientific, Inc.) and were allowed to aggregate into a single spheroid. After 48 h at 37˚C, the spheroids were embedded in a collagen hydrogel composed of DMEM supplemented with 5% FBS, 0.5% penicillin-streptomycin, and 2 mg/ml Cultrex 3D Culture Matrix Rat Collagen I (cat. no. 3447-020-01; R&D Systems, Inc.). Following gel polymerization, IGF-1 (50 μg/ml) was added to the culture medium. Spheroid sprouting was monitored, and images were captured 2 and 3 days after embedding using a Nikon Eclipse TS100 microscope (Nikon Corporation).

Quantification and bias control for Transwell and 3D invasion assays. Quantitative analysis of Transwell migration and 3D spheroid sprouting assays was performed using a blinded, back-to-back evaluation by two independent investigators. For Transwell assays, cells that invaded the bottom membrane were counted using ImageJ. For 3D spheroid assays, invasive sprouting was quantified by measuring protrusive areas emanating from the spheroid core. Each investigator analyzed the datasets independently, and the averaged values were used for statistical analysis. Inter-observer variability was minimal and did not affect the overall trends. This approach was implemented to minimize observer bias and ensure reproducibility.

Statistical analysis. All experiments were performed at least three times. Data are presented as the mean ± standard deviation. Statistical significance between two groups was assessed using a unpaired two-tailed Student's t-test. For comparisons involving more than two groups, one-way analysis of variance (ANOVA) followed by Sidak's or Dunnett's multiple-comparisons test or two-way ANOVA followed by Tukey's test was used. $P<0.05$ was considered to indicate a statistically significant difference. All analyses were performed using GraphPad Prism 10 (Dotmatics).

Results

IL-11 is notably expressed in RAS-mutated cancer cells and is induced by IGF-1 in pancreatic carcinoma cells. Steady-state levels of *IL11* mRNA in several human cancer cell lines were

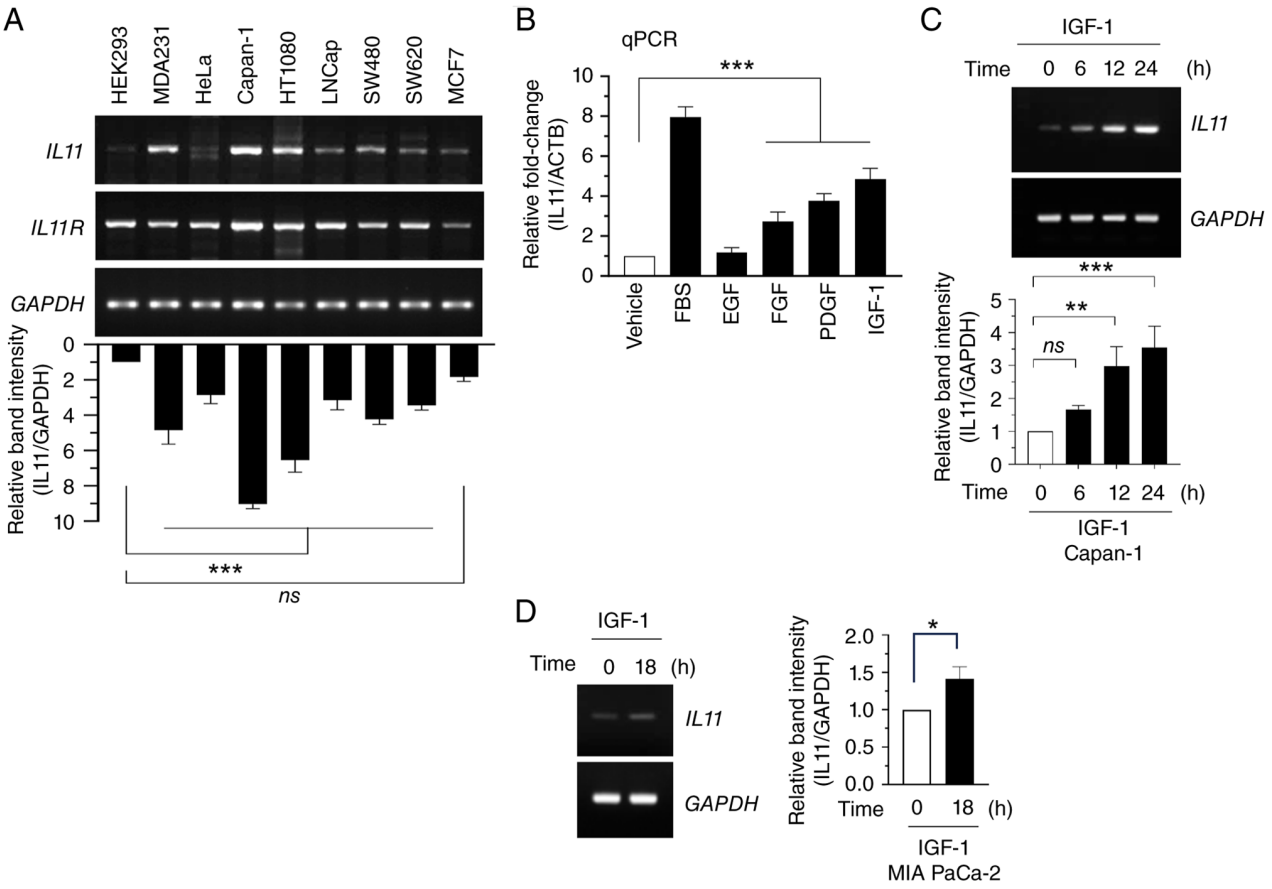

Figure 1. Steady-state levels of *IL11* mRNA in cancer cells and the stimulation of *IL11* induction by various growth factors in Capan-1 cells. (A) PCR analysis of *IL11* and *IL11R* mRNAs in various cancer cell lines. *GAPDH* mRNA was used as an internal control. Relative band intensities were normalized to *GAPDH* levels using ImageJ. Data are presented as mean ± SD (n=3). ***P<0.001 by Dunnett's multiple comparisons test. (B) qPCR of *IL11* mRNA in Capan-1 cells following stimulation with vehicle (PBS), 10% FBS, 20 ng/ml EGF, 50 ng/ml FGF, 50 ng/ml PDGF and 100 ng/ml IGF-1. *ACTB* was used as the endogenous control. Data are presented as mean ± SD (n=3). ***P<0.001 by one-way ANOVA followed Dunnett's multiple comparisons test. (C and D) PCR analysis of *IL11* mRNA in (C) Capan-1 and (D) MIA PaCa-2 cells treated with IGF-1 (100 ng/ml) for the indicated time periods. Relative band intensities were normalized to *GAPDH* levels using ImageJ. Data are presented as mean ± SD (n=3). *P<0.05, **P<0.01, ***P<0.001 by one-way ANOVA followed Dunnett's multiple-comparisons test. qPCR, quantitative PCR; ns, not significant; IGF-1, insulin-like growth factor 1; EGF, epidermal growth factor; FGF, fibroblast growth factor; PDGF, platelet-derived growth factor; FBS, fetal bovine serum.

examined by PCR. Consistent with a previous report (9), *IL11* mRNA was notably expressed in *RAS*-mutated cancer cells, including breast cancer cells (MDA-MB-231; *KRAS* G13D), pancreatic cancer cells (Capan-1; *KRAS* G12V), fibrosarcoma cells (HT1080; *NRAS* C181A) and colon cancer cells (SW480 and SW620; *KRAS* G12V), but not in cells harboring wild-type *RAS* (293, HeLa, MCF7) (Fig. 1A). Because *KRAS* mutations occur in >90% of pancreatic cancers (4), Capan-1 pancreatic carcinoma cells were selected to identify the IGF-1 response element within the *IL11* promoter region.

qPCR analysis revealed that multiple mitogens, including FBS, FGF, PDGF and IGF-1, significantly enhanced *IL11* expression in Capan-1 cells; however, EGF only had a minor effect (Fig. 1B). Based on these findings, IGF-1 was selected for further study. PCR analysis showed that treatment with 100 ng/ml IGF-1 increased *IL11* mRNA levels in Capan-1 in a time-dependent fashion (Fig. 1C). Consistently, IGF-1 also increased *IL11* mRNA expression in MIA PaCa-2 pancreatic cancer cells (Fig. 1D), indicating that this response is not restricted to a single cellular context. Subsequent mechanistic analyses were conducted primarily in Capan-1 cells, where *IL11* expression was relatively high among the tested cell lines.

Putative EBS functions as an IGF-1 response element in the IL11 promoter. Although *IL11* expression is driven by oncogenic RAS signaling through the AP-1 transcription factor, disruption of the AP-1 binding site alone within the promoter does not fully suppress *IL11* promoter activity (9), suggesting the involvement of additional cis-regulatory elements. JASPAR analysis identified a putative EBS located at -48 to -32 nucleotides (nt), adjacent to the AP-1 site spanning -99 to -87 nt (Fig. 2A).

Consistent with previous findings (9), site-directed mutation of the AP-1 binding site (mtAP-1) in the pIL11-Luc(-153/+14) construct significantly reduced IGF-1-induced *IL11* promoter activity. By contrast, mutation of the EBS (mtEBS) abolished promoter activity despite the presence of an intact AP-1 site (Fig. 2B). Moreover, co-transfection of an EGR1 expression vector with pIL11-Luc(-153/+14) significantly enhanced promoter-reporter activity (Fig. 2C). Notably, co-expression of EGR1 and FRA-1 resulted in an additive increase in promoter-reporter activity. These data suggest that the EBS functions as an active IGF-1 responsive cis-element and that cooperative regulation by EGR1 and AP-1 is required for maximal *IL11* transcription.

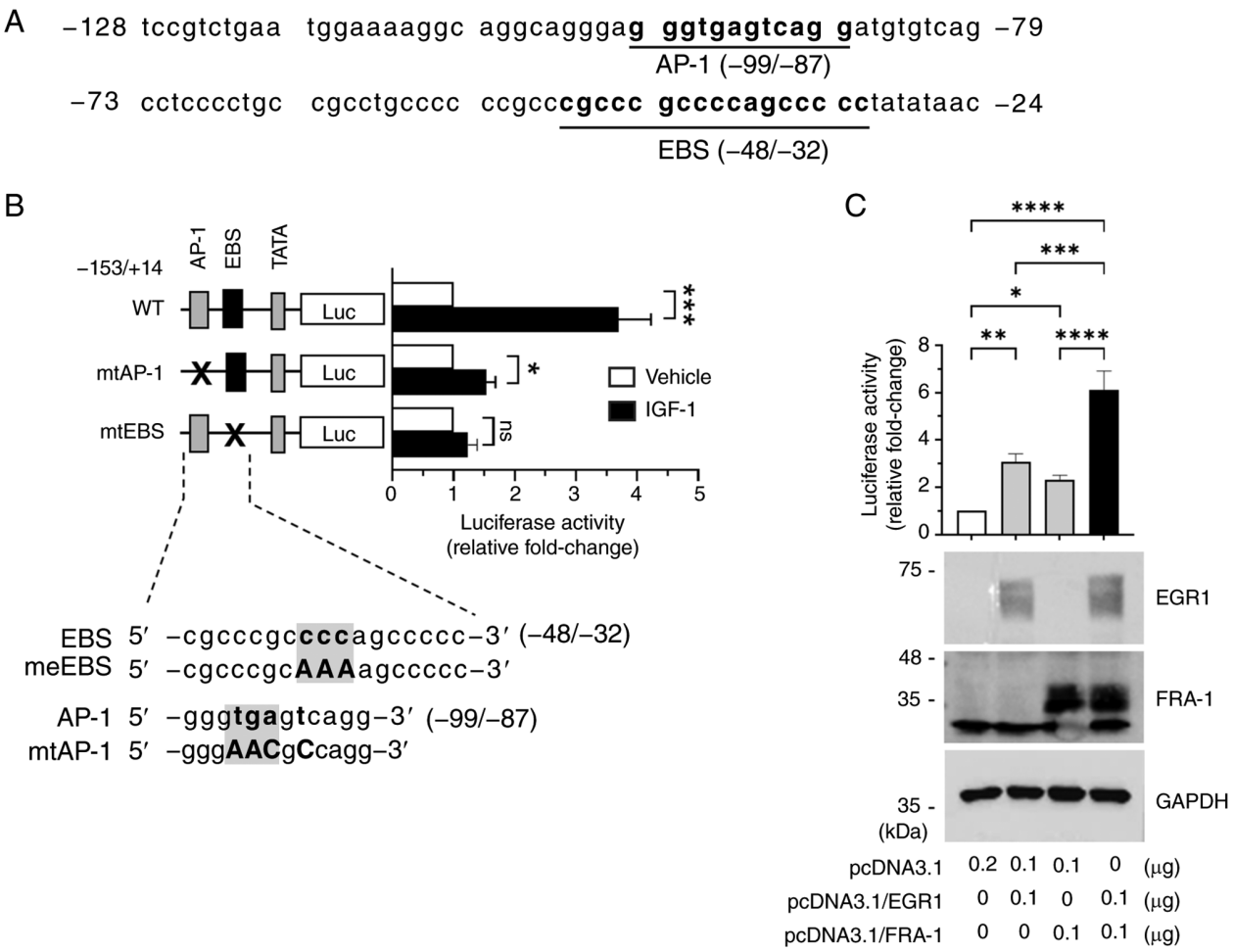

Figure 2. EBS is an IGF-1 response element. (A) EGR1-binding sequence (EBS) and AP-1-binding site in the *IL11* promoter region. (B) Capan-1 cells were transfected with 0.1 μg of WT, mtAP1 or mtEBS pIL11-Luc(-153/+14) promoter-reporter constructs. After 24 h, cells were treated with vehicle (PBS) or 100 ng/ml IGF-1 for an additional 12 h, and luciferase activity was measured. Data are presented as mean ± SD (n=3). *P<0.05, ***P<0.001 one-way ANOVA followed by Sidak's multiple comparisons test. (C) Capan-1 cells were co-transfected with pIL11-Luc(-153/+14) construct together with either an EGR1 or FRA-1 expression vector or both. After 48 h, the cells were harvested, and luciferase activity was measured. The immunoblot shown below the graph confirms the expression of the transfected EGR1 and FRA-1 proteins, with GAPDH serving as a loading control. Data are presented as mean ± SD (n=3). *P<0.05, **P<0.01, ***P<0.001, ****P<0.0001 one-way ANOVA followed by Dunnett's multiple-comparisons test. EGR1, early growth response 1; EBS, EGR1-binding sequence; IFG-1, insulin-like growth factor 1; mt, mutant; WT, wild-type; ns, not significant; FRA-1, Fos-related antigen 1.

EGR1 binds to the putative EBS site within the IL11 promoter. Because IGF-1 increased the expression of both EGR1 and the AP-1 component FRA-1 in Capan-1 (Fig. 3A) and MIA PaCa-2 cells (Fig. 3B), it was examined whether EGR1 directly binds to the *IL11* promoter using an EMSA. Purified recombinant EGR1 proteins bound to the EBS (Fig. 3C), confirming a direct interaction between EGR1 and the EBS within the *IL11* promoter. Nuclear extracts from IGF-1-treated MIA PaCa-2 cells formed specific DNA-protein complexes with the EBS probe (Fig. 3D). These findings demonstrate that IGF-1-induced EGR1 binds to the EBS site in the *IL11* promoter.

Silencing of EGR1 attenuates IGF-1-induced IL-11 expression. To further investigate the functional role of EGR1 in IGF-1-induced IL-11 expression, *EGR1* was silenced in Capan-1 cells using RNA interference. To validate the efficiency of EGR1 silencing, immunoblot analysis was performed in shEgr1-transfected cells. EGR1 protein levels were markedly reduced compared with the shCT control group (Fig. 4A). Densitometric analysis revealed an ~90% decrease in IGF-1-induced EGR1 expression in shEgr1 cells compared with shCT cells. This result demonstrates efficient knockdown of EGR1 at the protein level. PCR analysis showed a marked reduction in IGF-1-induced *IL11* mRNA expression in shEgr1 cells compared with shCT cells (Fig. 4B). Consistently, qPCR analysis demonstrated that IGF-1 treatment for 24 h increased *IL11* mRNA levels by 5.47-fold in shCT cells; by contrast, only a 1.73-fold increase was observed in shEgr1 cells relative to vehicle (PBS)-treated shCT cells (Fig. 4C). In agreement with these mRNA results, IGF-1-induced secretion of IL-11 protein into the culture medium was significantly reduced in shEgr1 cells compared with shCT cells (1.73 vs. 4.33 ng/ml) (Fig. 4D). Together, these findings support a role for EGR1 in the transcriptional regulation of *IL11* in response to IGF-1 stimulation.

To define the upstream signaling pathways governing IGF-1-induced EGR1 activation, Capan-1 cells were treated with MAPK signaling inhibitors. Treatment with the MEK/ERK inhibitor (10 μM U0126), the p38 kinase inhibitor (10 μM SB203580) or the JNK inhibitor (10 μM SP600125) significantly attenuated IGF-1-induced EGR1 protein

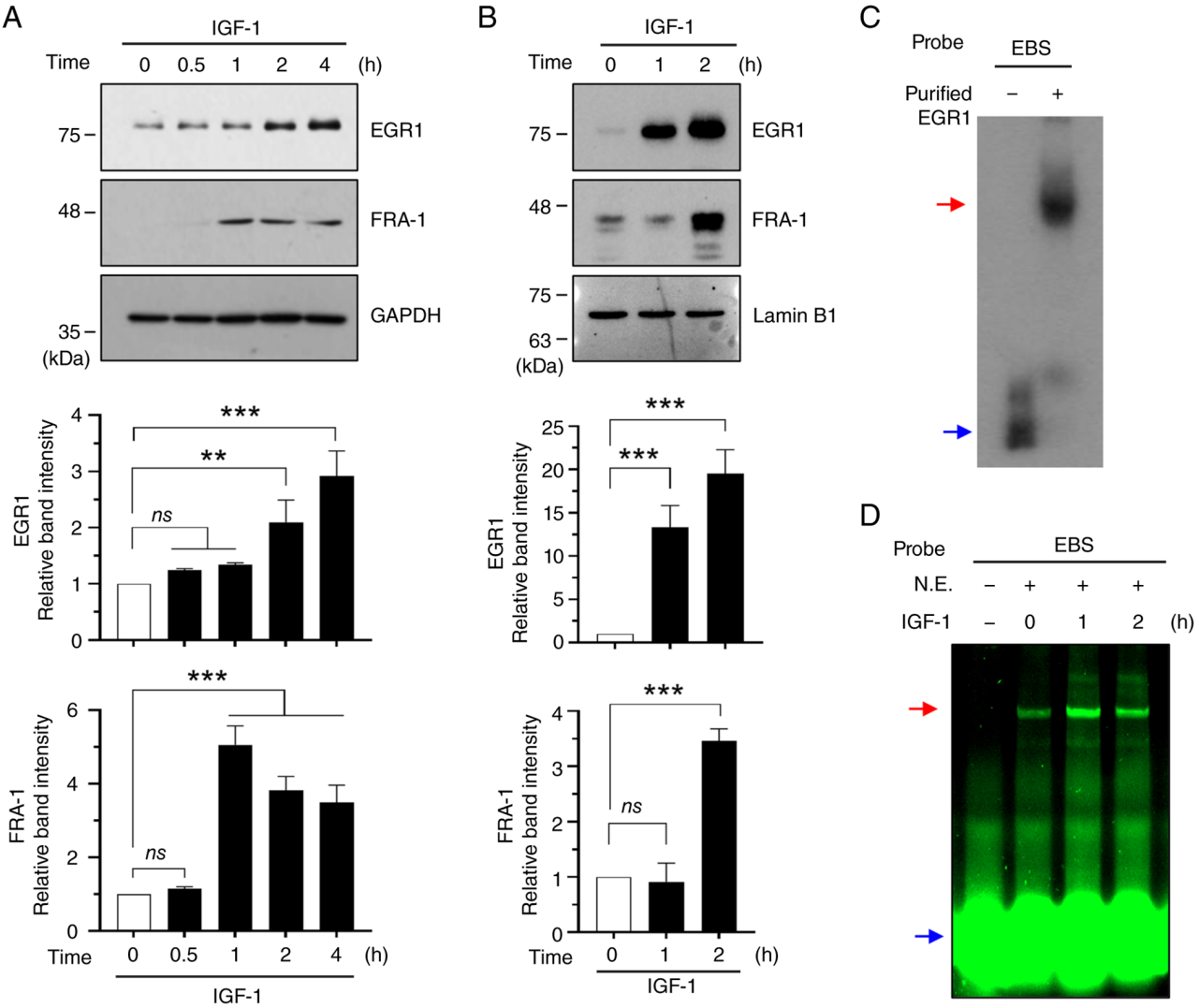

Figure 3. EGR1 binds to the EBS site in the *IL11* promoter. (A) Capan-1 and (B) MIA PaCa-2 cells were treated with IGF-1 (100 ng/ml) for different time periods. Immunoblotting was conducted using (A) whole lysates or (B) nuclear fraction. GAPDH and Lamin B1 served as markers for the cytosol and nucleus, respectively. Relative band intensities corresponding to each EGR1 or FRA-1 were measured using ImageJ (bottom graphs). Data are presented as mean ± SD (n=3). **P<0.01, ***P<0.001 one-way ANOVA followed by Dunnett's multiple-comparisons test. (C) Purified recombinant EGR1 proteins were incubated with a biotinylated EBS probe. (D) MIA PaCa-2 cells were treated with IGF-1 (100 ng/ml) for 1 or 2 h. Nuclear extracts (3 μg) were incubated with a 5'-6-FAM-labeled double-stranded EBS oligonucleotide probe. DNA-protein complexes were analyzed using a 6% non-denaturing polyacrylamide gel under native conditions. Fluorescent signals were detected using a ChemiDoc imaging system set to detect Alexa Fluor 488. The red arrow points to the DNA-protein complex, whereas the blue arrow points to the free oligonucleotide probe. N.E., nuclear extract; EGR1, early growth response 1; EBS, EGR1-binding sequence; IFG-1, insulin-like growth factor 1; FRA-1, Fos-related antigen 1; ns, not significant.

expression, as determined by immunoblotting (Fig. 4E). Consistently, qPCR analysis demonstrated that *IL11* mRNA induction by IGF-1 was significantly reduced under these conditions (Fig. 4F). These findings suggest that MAPK signaling coordinately regulates both EGR1 induction and AP-1 activation, thereby enabling cooperative transcriptional activation at the *IL11* promoter.

IGF-1/EGR1/IL-11 axis promotes IGF-1-induced invasion of pancreatic carcinoma cells. Finally, it was examined whether IL-11 functions as a downstream effector mediating the pro-invasive effects of IGF-1. An invasion assay using extracellular matrix-mimetic gel-coated inserts demonstrated that invasive motility of Capan-1 cells was increased following IGF-1 or IL-11 treatment (Fig. 5A, left panels). Quantitation of invaded cells revealed that IGF-1 treatment significantly increased the invasive area (27.03 pixels) compared with the vehicle control (2.606 pixels), representing an ~10-fold increase in invasive capability (Fig. 5A, right graph). Similarly, IL-11 treatment also enhanced cell invasion (11.99 pixels), albeit to a lesser extent than IGF1. To determine whether IGF1-induced invasion is mediated by IL-11 signaling, cells were co-treated with IGF-1 and a neutralizing antibody against the IL-11 receptor (αIL11R). Notably, the stimulatory effect of IGF-1 was significantly attenuated by IL-11R neutralization, with the invasive area decreasing to 4.827 pixels (~82% reduction compared with the IGF-1-only group). These findings suggest that the IGF-1-induced invasive phenotype is notably dependent on the activation of the IL-11/IL11R signaling axis.

To evaluate the functional role of EGR1 in IGF-1-induced invasive behavior, a three-dimensional (3D) spheroid sprouting assay was performed using Capan-1 transfectants (shCT and

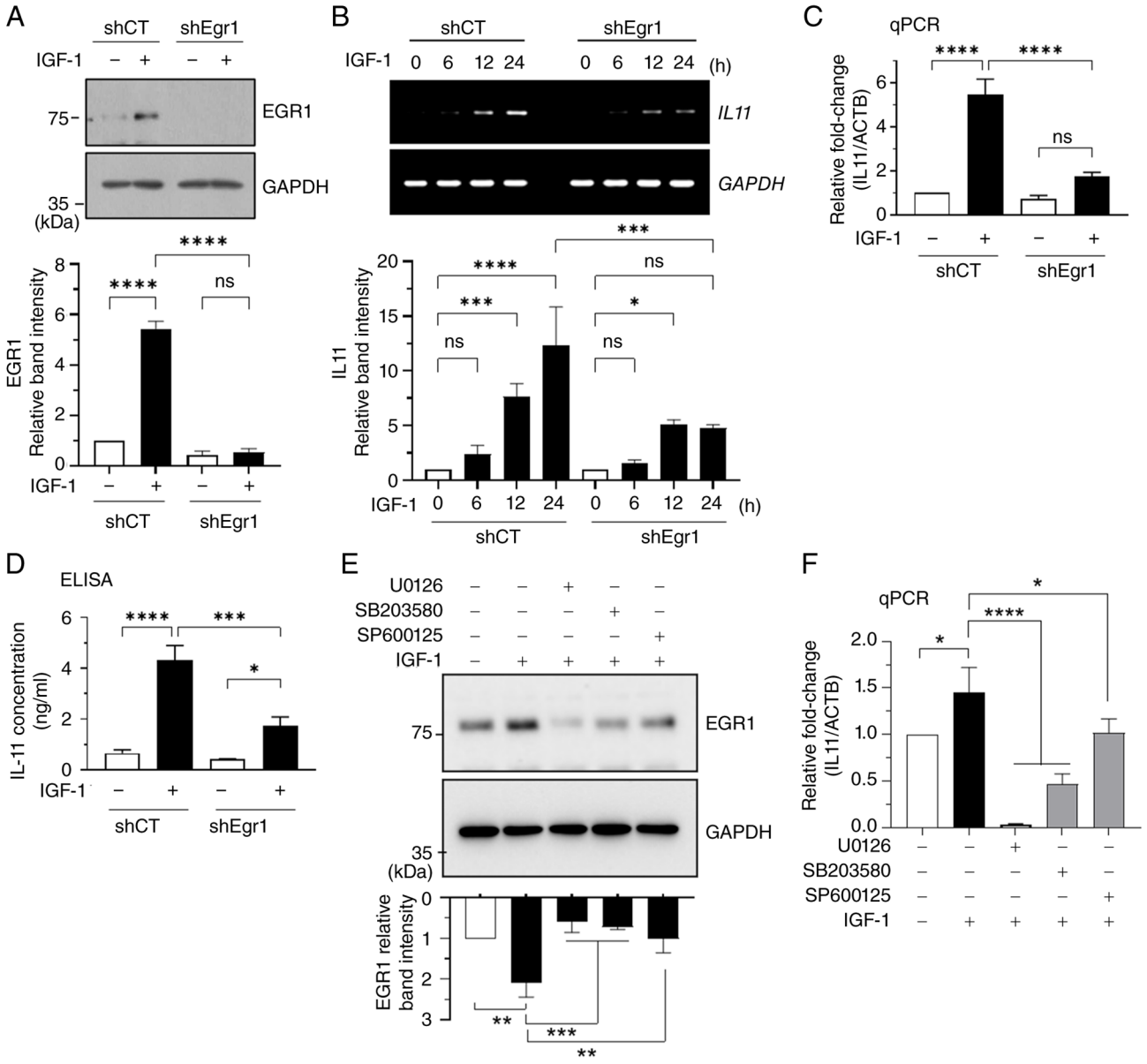

Figure 4. Impact of EGR1 silencing on suppressing IGF-1-induced *IL11* expression. (A) Capan-1 transfectants expressing scrambled control (shCT) or *EGR1* shRNA (shEgr1) were treated with IGF-1 (100 ng/ml) for 30 min. EGR1 protein levels were assessed by immunoblotting. GAPDH served as a loading control. Relative band intensities corresponding to EGR1 protein were measured using ImageJ (bottom graphs). Data are presented as mean ± SD (n=3). ns, not significant; ****P<0.0001 by two-way ANOVA followed by Tukey's multiple comparisons test. (B) shCT and shEgr1 cells were treated with IGF-1 (100 ng/ml) for the indicated time periods. Total RNA was isolated, and *IL11* mRNA expression was analyzed by PCR. Data are presented as mean ± SD (n=3). ns, not significant; *P<0.05, ***P<0.001; ****P<0.0001 by two-way ANOVA followed by Tukey's multiple comparisons test. (C) qPCR. shCT and shEgr1 cells were treated with IGF-1 (100 ng/ml) for 24 h. *IL11* mRNA levels were quantified using the $2^{-\Delta\Delta Cq}$ method with *ACTB* as the endogenous control. Data are presented as mean ± SD (n=3). ns, not significant, ****P<0.0001 by two-way ANOVA followed by Tukey's multiple comparisons test. (D) ELISA. Cells were treated as in (C). IL-11 levels secreted into the culture medium were quantified using a solid-phase sandwich ELISA method. Data are presented as mean ± SD (n=3). *P<0.05, ***P<0.001; ****P<0.0001 by two-way ANOVA followed by Tukey's multiple comparisons test. (E) Capan-1 cells were pre-treated with 10 μM U0126, 10 μM SB203580 or 10 μM SP600125 for 30 min before stimulating IGF-1 (100 ng/ml). After 90 min, cells were collected, and immunoblotting was performed with GAPDH as an internal control. Relative band intensities corresponding to each EGR1 was measured using ImageJ (bottom graphs). Data are presented as mean ± SD (n=3). **P<0.01, ***P<0.001 by Dunnett's multiple-comparisons test. (F) Capan-1 cells were pre-treated with MAPK inhibitors and IGF-1 as in (E). After 18 h, cells were collected, and qPCR (was performed with *ACTB* as an internal control. Data are presented as mean ± SD (n=3). *P<0.05, ****P<0.0001 by one-way ANOVA followed by Sidak's multiple comparisons test. IFG-1, insulin-like growth factor 1; EGR1, early growth response 1; shCT, short hairpin RNA control; shEGR1, short hairpin RNA EGR1; ns, not significant; qPCR, quantitative PCR.

shEgr1). The spheroids were embedded in a collagen hydrogel prepared using Cultrex 3D Culture Matrix Rat Collagen I. Under basal conditions, control spheroids (shCT) maintained a compact, well-circumscribed architecture with minimal outward cell migration (Fig. 5B, left panels). Upon IGF-1 stimulation, shCT spheroids exhibited pronounced invasive outgrowths characterized by irregular, radially oriented protrusions extending into the surrounding matrix, consistent with increased invasive capacity. These protrusions frequently appeared as multicellular extensions with variable length and thickness, reflecting enhanced cellular dissemination from the spheroid core. By contrast, EGR1-silenced spheroids (shEgr1)

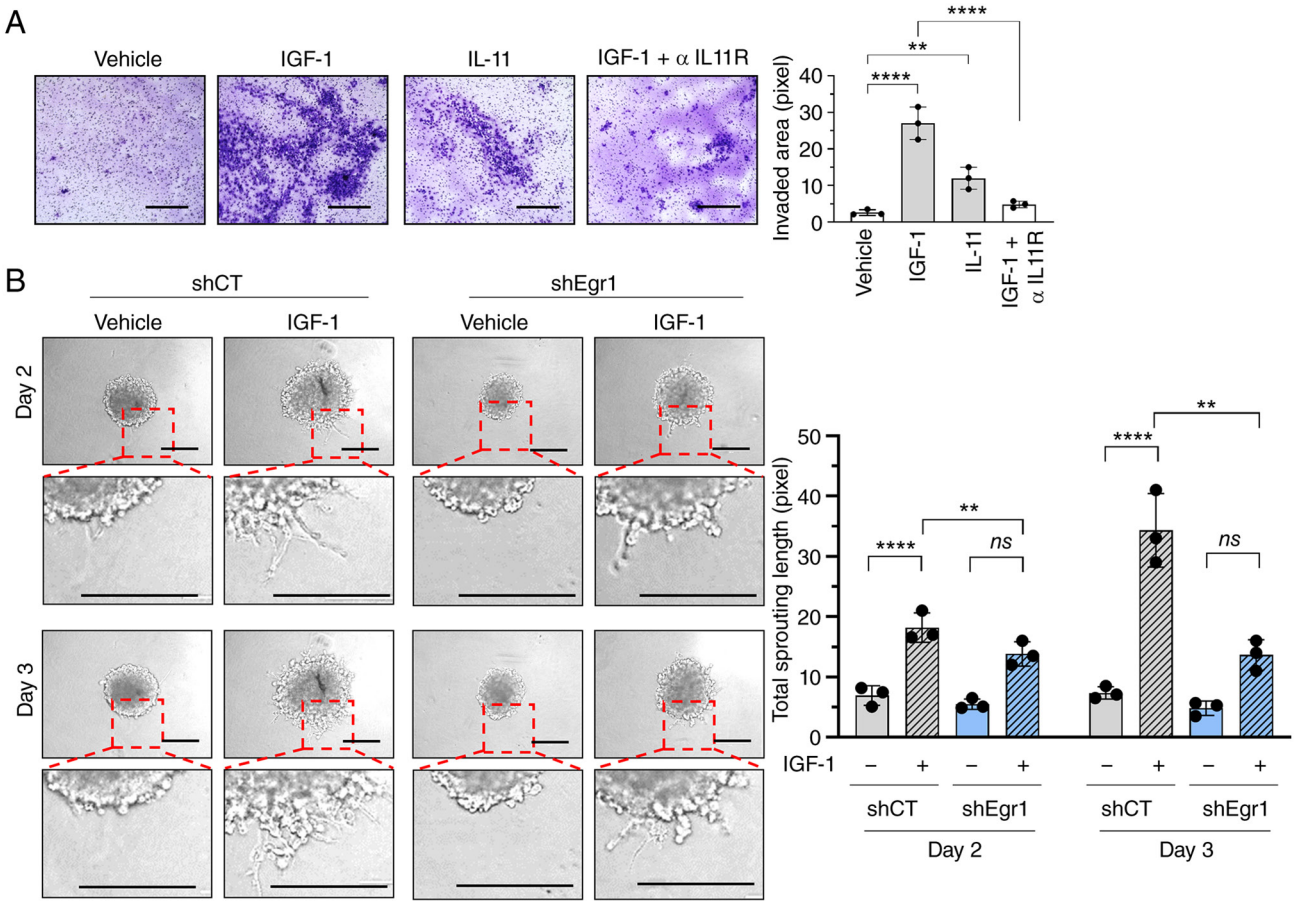

Figure 5. Role of EGR1/IL-11 signaling axis in promoting IGF-1-induced invasive motility in Capan-1 cells. (A) Transwell invasion assay. Capan-1 cells in serum-free medium were seeded onto the upper chamber of the insert and treated with IGF-1 (100 ng/ml), IL-11 (10 ng/ml) or IGF-1 with neutralizing antibody to IL11Rα (2 μg/ml). After 24 h, invasive cells that passed through the membrane and migrated to the bottom of the insert were stained with 0.1% crystal violet. The invaded area (pixels) was quantified by calculating the integrated density of stained cells using ImageJ. Scale bar, 100 μm. Data are presented as the mean ± SD (n=3) of three independent experiments. **P<0.01, ****P<0.0001 by one-way ANOVA followed by Sidak's multiple comparisons test. (B) 3D spheroid sprouting assay. Capan-1 transfectants, shCT and shEgr1 cells, were cultured as three-dimensional spheroids and were treated with IGF-1 (100 ng/ml) for 2 or 3 days in a Matrigel-based extracellular matrix. Invasive protrusions were captured using a Nikon Eclipse TS100 microscope. The invasion capability was quantified by measuring the length of outward sprouts. Quantification was performed by two independent investigators using ImageJ in a blinded, back-to-back manner, and averaged values were used for statistical analysis. Data are presented as mean ± SD (n=3) from three independent experiments. **P<0.01, ****P<0.0001 by two-way ANOVA with Tukey's multiple comparisons test. Scale bar, 400 μm. IFG-1, insulin-like growth factor 1; EGR1, early growth response 1; shCT, short hairpin RNA scrambled control; shEGR1, short hairpin RNA EGR1; ns, not significant; IL-11, interleukin 11; IL11R, IL-11 receptor; ns, not significant.

displayed a markedly attenuated invasive phenotype following IGF-1 treatment, retaining a relatively compact morphology with a significant reduction in total length of outward sprouts by ~59.7% at day 2 and 60.2% at day 3 compared with control spheroids (Fig. 5B, right graph). These findings indicate that EGR1 contributes to the morphological transition from a confined spheroid architecture to an invasive growth pattern in response to IGF-1 stimulation. Collectively, these results support a model in which the IGF-1/EGR1/IL11 axis promotes invasion, although the precise cellular mechanisms, including potential EMT involvement and invasion mode, remain to be defined.

Discussion

The aggressive clinical behavior of pancreatic cancer is closely linked to its capacity to invade surrounding tissues and metastasize to distant organs (21). In the present study, a signaling pathway was identified that connects growth factor stimulation to the invasive behavior of pancreatic cancer cells. IGF-1 induces the expression of the immediate-early transcription factor EGR1, which in turn promotes IL-11 expression and secretion. Functionally, IL-11 acts as a downstream effector that mediates the pro-invasive effects of IGF-1. The present findings provide mechanistic insight into the upstream regulation of EGR1 in response to IGF-1. Pharmacological inhibition of MEK/ERK, p38 and JNK pathways collectively attenuated EGR1 induction, indicating that EGR1 activation is not governed by a single dominant cascade but instead reflects integrated MAPK signaling. Notably, suppression of IL-11 expression under these conditions supports a model in which MAPK-dependent EGR1 activation serves as a notable transcriptional node linking IGF-1 signaling to IL-11 expression. This multi-pathway dependency may explain the robust and sustained induction of IL-11 observed in the tumor context. Collectively, these findings define an IGF-1/EGR1/IL-11 signaling axis that contributes to the invasive phenotype of pancreatic cancer and reveal a previously

uncharacterized mechanism linking IGF-1 signaling to cytokine-driven invasion.

The pro-tumorigenic role of IGF-1 signaling is well established (3,22); however, the specific downstream effectors mediating IGF-1-driven invasion in pancreatic cancer remain incompletely defined. A key finding of the present study is the identification of IL-11 as a functionally important downstream effector of the IGF-1/EGR1 signal axis. IL-11 is a member of the IL-6 family of cytokines, which are widely recognized for their roles in cancer-associated inflammation and tumor progression (23). The present data support a model in which IGF-1 activates an EGR1/IL-11 signaling cascade to promote invasive behavior, consistent with emerging evidence implicating this pathway in metastatic progression (24). EGR1 functions as a transcriptional hub that integrates diverse extracellular cues and orchestrates coordinated cellular responses to environmental stimuli. Previous studies have reported that EGR1 exhibits context-dependent roles in cancer, functioning as a tumor suppressor in certain cancer types by inducing pro-apoptotic or growth-inhibitory genes. For instance, EGR1 can induce growth arrest and apoptosis by transcriptionally activating tumor suppressor genes such as *TP53* and *PTEN*, in glioblastoma and hematologic malignancies (25,26). However, accumulating evidence also supports a pro-tumorigenic role for EGR1, particularly in response to growth factor-mediated signaling (15). Although EGR1 has been reported to exert context-dependent roles in cancer (27), the present findings implicate EGR1 as a pro-invasive regulator, linking upstream growth factor signaling to activation of an invasion-associated gene program in pancreatic cancer, suggesting that EGR1 may act as a context-dependent regulator that favors tumor progression under specific microenvironmental and signaling conditions.

Cancer cell invasion is closely associated with EMT, a hallmark of cellular plasticity that confers migratory and invasive properties (28). Both IGF-1 signaling and IL-6 family cytokines have been implicated in EMT induction (29,30). The 3D spheroid invasion assay provides functional support for a role of EGR1 in mediating IGF-1-driven invasive behavior in pancreatic cancer cells. IGF-1 stimulation induced a marked transition from a compact, well-circumscribed spheroid architecture to an invasive growth pattern characterized by irregular, radially oriented multicellular protrusions extending into the extracellular matrix. Such morphological changes are widely interpreted as features of enhanced invasive capacity in 3D culture systems (31). Notably, silencing of EGR1 substantially attenuated these invasive outgrowths, preserving a more confined spheroid morphology despite IGF-1 stimulation. These findings suggest that EGR1 functions as a notable downstream effector of IGF-1 signaling to promote invasive phenotypes, consistent with its role in transcriptionally activating *IL11* identified in the present study. Given that IL-11 has been implicated in tumor-stromal interactions and pro-invasive signaling (2), the observed morphological changes may reflect a transcriptionally driven reprogramming of tumor cell behavior downstream of the IGF-1/EGR1/IL11 axis. However, while the invasion patterns observed in the present study are consistent with increased cellular motility and matrix interaction, the present study does not distinguish between collective and individual modes of invasion, nor does it directly assess EMT-associated molecular changes. Future studies incorporating high-resolution imaging and EMT marker analysis, including E-cadherin, N-cadherin, Slug and Vimentin, as well as EMT-associated transcriptional networks, will be necessary to define the precise cellular mechanisms underlying EGR1-dependent invasion in pancreatic cancer.

From a therapeutic perspective, the present findings suggest that targeting downstream transcriptional regulators such as EGR1 may provide a strategy to selectively inhibit invasion-associated gene programs while preserving upstream growth factor signaling. Although small-molecule inhibitors targeting EGR1 have been described (12), their efficacy in suppressing pancreatic cancer invasion and metastasis remains to be determined. Future investigations should assess whether these agents, alone or in combination with inhibitors of related oncogenic pathways, can effectively limit metastatic progression and improve therapeutic outcomes in pancreatic cancer.

The present study had several limitations. Detailed mechanistic analyses of the IGF-1/EGR1/IL11 axis were performed primarily in Capan-1 cells. Although IGF-1-induced IL-11 expression was reproducibly observed in both Capan-1 and MIA PaCa-2 cells, indicating that the downstream transcriptional output is conserved, the extent to which EGR1-dependent regulatory mechanisms are uniformly maintained across diverse PDAC contexts remains to be determined. Further research using more cell lines and *in vivo* models will be required to validate the applicability of this signaling pathway. Furthermore, 2D cultures and 3D spheroid models provide valuable mechanistic insight; however, they do not fully recapitulate the complexity of tumor behavior *in vivo*. Accordingly, future studies should validate these findings in more physiologically relevant systems, including patient-derived organoids, xenograft models, and genetically engineered mouse models.

Although the present study provides mechanistic insight into the IGF-1-EGR1-IL11 axis in pancreatic cancer cells, validation in clinical PDAC specimens will be required to establish its translational relevance. Future studies incorporating immunohistochemical analysis of patient-derived tissues will be necessary to determine whether EGR1 and IL-11 are co-expressed at the invasive front and whether their expression is associated with clinicopathological parameters, including tumor grade, perineural invasion and lymph node metastasis. Such analyses would further strengthen strengthening the translational relevance of the IGF-1/EGR1/IL-11 signaling axis. PDAC is characterized by a dense desmoplastic stroma (32), in which cancer-associated fibroblasts (CAFs) serve as a major source of cytokines, including IL-11 (33). While the present study defines a tumor cell-intrinsic mechanism whereby IGF-1-induced EGR1 drives *IL11* transcription and promotes invasive behavior, it does not account for paracrine contributions from stromal components. *In vivo*, CAF-derived IL-11 may act in concert with tumor cell-derived IL-11 to amplify pro-invasive signaling within the tumor microenvironment. Therefore, future studies incorporating co-culture systems or stromal modeling approaches will be necessary to delineate the relative contributions of autocrine and paracrine IL-11 signaling in PDAC progression.

In addition to its role in promoting invasive behavior, EGR1 has been implicated in other key tumor characteristics, including proliferation and chemotherapeutic response. Previous studies have demonstrated that EGR1 contributes to gemcitabine resistance in pancreatic cancer by enhancing cell survival and attenuating apoptosis, as well as by mediating adaptive transcriptional responses under therapeutic stress (34-36). These findings suggest that EGR1 may regulate multiple aspects of tumor progression beyond invasion. Although the present study primarily focused on the IGF-1/EGR1/IL-11 axis in regulating invasive behavior, it is possible that this signaling pathway may also influence proliferative capacity and drug sensitivity. Further investigation will be required to elucidate the role of EGR1 in proliferation and chemoresistance, particularly in the context of gemcitabine treatment.

To further explore the potential clinical relevance of the present findings, overall survival data from the TCGA PAAD cohort available through the UCSC Xena Browser (https://xenabrowser.net/datapages/) was independently analyzed. This analysis showed that patients with high expression of both EGR1 and IL11 had poorer overall survival than those with low expression of both genes. Although this observation does not establish a causal relationship, it is consistent with the present experimental findings and supports the potential clinical relevance of the EGR1-IL-11 regulatory axis in PDAC progression.

In summary, IGF-1 rapidly induces EGR1, which engages the *IL11* promoter and may function in conjunction with AP-1-associated transcriptional activity, including FRA-1, to enhance *IL11* transcription. Establishing the precise nature of this relationship would require additional experiments, such as co-immunoprecipitation, sequential chromatin immunoprecipitation (ChIP)-reChIP assay, or *in situ* proximity ligation assay, to demonstrate direct physical or functional cooperation. Genetic silencing of EGR1 markedly attenuated IL-11 production and suppressed IGF-1-induced invasion, thereby linking growth factor-dependent transcriptional regulation to invasive behavior. Given the high prevalence of *KRAS* mutations and the frequent activation of IGF-1 signaling in pancreatic cancer, the IGF-1-EGR1-IL-11 axis may represent a promising therapeutic target. Future studies should determine whether pharmacologic disruption of this pathway can effectively limit the invasive and metastatic progression in pancreatic cancer.

Acknowledgements

The present study was supported by the Konkuk University Research Professor Program.

Funding

The present study was supported by a National Research Foundation of Korea grant funded by the Korean Government (grant no. 2023R1A2C1003601).

Availability of data and materials

The data generated in the present study may be requested from the corresponding author.

Authors' contributions

YC, EJ and JH performed the statistical analyses, functional investigations, and additional experiments during manuscript revision. YC and EJ wrote the original draft of the manuscript. YC and EJ confirm the authenticity of all the raw data. SYS conceived and supervised the study, provided the financial support, and reviewed and edited the manuscript. All the authors have read and approved the final version of the manuscript.

Ethics approval and consent to participate

Not applicable.

Patient consent for publication

Not applicable.

Competing interests

The authors declare that they have no competing interests.

References

1. Schindler C, Levy DE and Decker T: JAK-STAT signaling: From interferons to cytokines. J Biol Chem 282: 20059-20063, 2007.
2. Johnstone CN, Chand A, Putoczki TL and Ernst M: Emerging roles for IL-11 signaling in cancer development and progression: Focus on breast cancer. Cytokine Growth Factor Rev 26: 489-498, 2015.
3. Xu DH, Zhu Z, Wakefield MR, Xiao H, Bai Q and Fang Y: The role of IL-11 in immunity and cancer. Cancer Lett 373: 156-163, 2016.
4. Punekar SR, Velcheti V, Neel BG and Wong KK: The current state of the art and future trends in RAS-targeted cancer therapies. Nat Rev Clin Oncol 19: 637-655, 2022.
5. Sharma R, Kumar S, Ghosh R, Komal K and Kumar M: Gene therapy: Transforming the battle against pancreatic cancer. Curr Gene Ther 26: 152-159, 2025.
6. Tian G, Liu C, Che C, Ren S, Zhang K, Zhou P, Wang K, Lu G, Xia Y, Wang Y, *et al*: Identifying ARRB2 as a prognostic biomarker and key player in the tumor microenvironment of pancreatic cancer through scPagwas methodology. Curr Gene Ther 26: 203-222, 2025.
7. Ipek SL, Alkıs MDO, Tulek A and Gokturk D: Recombinant expression of l-methioninase from brevibacterium linens and evaluation of its anticarcinogenic properties against MiaPaCa-2 cells. Protein Pept Lett 32: 451-464, 2025.
8. Pollak M: Insulin and insulin-like growth factor signalling in neoplasia. Nat Rev Cancer 8: 915-928, 2008.
9. Shin SY, Choi C, Lee HG, Lim Y and Lee YH: Transcriptional regulation of the interleukin-11 gene by oncogenic Ras. Carcinogenesis 33: 2467-2476, 2012.
10. Rauluseviciute I, Riudavets-Puig R, Blanc-Mathieu R, Castro-Mondragon JA, Ferenc K, Kumar V, Lemma RB, Lucas J, Chèneby J, Baranasic D, *et al*: JASPAR 2024: 20th anniversary of the open-access database of transcription factor binding profiles. Nucleic Acids Res 52: D174-D182, 2024.
11. Hoffmann E, Ashouri J, Wolter S, Doerrie A, Dittrich-Breiholz O, Schneider H, Wagner EF, Troppmair J, Mackman N and Kracht M: Transcriptional regulation of EGR-1 by the interleukin-1-JNK-MKK7-c-Jun pathway. J Biol Chem 283: 12120-12128, 2008.
12. Yeo H, Ahn SS, Lee JY, Jung E, Jeong M, Kang GS, Ahn S, Lee Y, Koh D, Lee YH, *et al*: Disrupting the DNA binding of EGR-1 with a small-molecule inhibitor ameliorates 2, 4-dinitrochlorobenzene-induced skin inflammation. J Invest Dermatol 141: 1851-1855, 2021.
13. Shin SY, Lee JM, Lim Y and Lee YH: Transcriptional regulation of the growth-regulated oncogene alpha gene by early growth response protein-1 in response to tumor necrosis factor α stimulation. Biochim Biophys Acta 1829: 1066-1074, 2013.

14. Zou K and Zeng Z: Role of early growth response 1 in inflammation-associated lung diseases. Am J Physiol Lung Cell Mol Physiol 325: L143-L154, 2023.
15. Wang B, Guo H, Yu H, Chen Y, Xu H and Zhao G: The role of the transcription factor EGR1 in cancer. Front Oncol 11: 642547, 2021.
16. Yan SF, Fujita T, Lu J, Okada K, Shan Zou Y, Mackman N, Pinsky DJ and Stern DM: Egr-1, a master switch coordinating upregulation of divergent gene families underlying ischemic stress. Nat Med 6: 1355-1361, 2000.
17. Fahmy RG, Dass CR, Sun LQ, Chesterman CN and Khachigian LM: Transcription factor Egr-1 supports FGF-dependent angiogenesis during neovascularization and tumor growth. Nat Med 9: 1026-1032, 2003.
18. Yeo H, Ahn SS, Lee YH and Shin SY: Regulation of pro-opiomelanocortin (POMC) gene transcription by interleukin-31 via early growth response 1 (EGR-1) in HaCaT keratinocytes. Mol Biol Rep 47: 5953-5962, 2020.
19. Livak KJ and Schmittgen TD: Analysis of relative gene expression data using real-time quantitative PCR and the 2(-Delta Delta C(T)) method. Methods 25: 402-408, 2001.
20. Jung E, Ou S, Ahn SS, Yeo H, Lee YH and Shin SY: The JNK-EGR1 signaling axis promotes TNF-alpha-induced endothelial differentiation of human mesenchymal stem cells via VEGFR2 expression. Cell Death Differ 30: 356-368, 2023.
21. Joshi VB, Ruiz OL and Razidlo GL: The cell biology of metastatic invasion in pancreatic cancer: Updates and mechanistic insights. Cancers 15: 2169, 2023.
22. Liu G, Zhu M, Zhang M and Pan F: Emerging role of IGF-1 in prostate cancer: A promising biomarker and therapeutic target. Cancers (Basel) 15: 1287, 2023.
23. Soler MF, Abaurrea A, Azcoaga P, Araujo AM and Caffarel MM: New perspectives in cancer immunotherapy: Targeting IL-6 cytokine family. J Immunother Cancer 11: e007530, 2023.
24. Wang P, Mak VC and Cheung LW: Drugging IGF-1R in cancer: New insights and emerging opportunities. Genes Dis 10: 199-211, 2023.
25. Virolle T, Adamson ED, Baron V, Birle D, Mercola D, Mustelin T and de Belle I: The Egr-1 transcription factor directly activates PTEN during irradiation-induced signalling. Nat Cell Biol 3: 1124-1128, 2001.
26. Krones-Herzig A, Mittal S, Yule K, Liang H, English C, Urcis R, Soni T, Adamson ED and Mercola D: Early growth response 1 acts as a tumor suppressor in vivo and in vitro via regulation of p53. Cancer Res 65: 5133-5143, 2005.
27. Li TT, Liu MR and Pei DS: Friend or foe, the role of EGR-1 in cancer. Med Oncol 37: 7, 2019.
28. Brabletz S, Schuhwerk H, Brabletz T and Stemmler MP: Dynamic EMT: A multi-tool for tumor progression. EMBO J 40: e108647, 2021.
29. Abaurrea A, Araujo AM and Caffarel MM: The role of the IL-6 cytokine family in epithelial-mesenchymal plasticity in cancer progression. Int J Mol Sci 22: 8334, 2021.
30. Cevenini A, Orrù S, Mancini A, Alfieri A, Buono P and Imperlini E: Molecular signatures of the insulin-like growth factor 1-mediated epithelial-mesenchymal transition in breast, lung and gastric cancers. Int J Mol Sci 19: 2411, 2018.
31. Friedl P and Wolf K: Plasticity of cell migration: A multiscale tuning model. J Cell Biol 188: 11-19, 2010.
32. Neesse A, Bauer CA, Öhlund D, Lauth M, Buchholz M, Michl P, Tuveson DA and Gress TM: Stromal biology and therapy in pancreatic cancer: Ready for clinical translation? Gut 68: 159-171, 2019.
33. Kalluri R: The biology and function of fibroblasts in cancer. Nat Rev Cancer 16: 582-598, 2016.
34. Chen C, Zhao S, Zhao X, Cao L, Karnad A, Kumar AP and Freeman JW: Gemcitabine resistance of pancreatic cancer cells is mediated by IGF1R dependent upregulation of CD44 expression and isoform switching. Cell Death Dis 13: 682, 2022.
35. Bangbo Z, Cheng Q, Zeru L, Tianyu L, Yutong Z, Weibin W and Yupei Z: RNA binding protein Pumilio2 promotes chemoresistance of pancreatic cancer via focal adhesion pathway and interacting with transcription factor EGR1. Cell Mol Life Sci 82: 78, 2025.
36. Zhang JF, Tao LY, Yang MW, Xu DP, Jiang SH, Fu XL, Liu DJ, Huo YM, Liu W, Yang JY, *et al*.: CD74 promotes perineural invasion of cancer cells and mediates neuroplasticity via the AKT/EGR-1/GDNF axis in pancreatic ductal adenocarcinoma. Cancer Lett 508: 47-58, 2021.